



Effect of reaction media on hydrogenolysis of polyethylene plastic waste: Polymer-surface interactions in small alkane/polymer blends

Mehdi Zare ^a, Pavel A. Kots ^a, Zachary R. Hinton ^a, Thomas H. Epps, III ^{a,b,c}, LaShanda T. J. Korley ^{a,b,c}, Stavros Caratzoulas ^{a,*}, Dionisios G. Vlachos ^{a,b,*}

^a Center for Plastics Innovation, University of Delaware, 221 Academy Street, Newark, DE 19716, United States

^b Department of Chemical and Biomolecular Engineering, University of Delaware, 150 Academy Street, Newark, DE 19716, United States

^c Department of Materials Science and Engineering, University of Delaware, 127 The Green, Newark, DE 19716, United States

ARTICLE INFO

Keywords:

Plastic waste
Polyethylene
Multiscale simulation
Solvent effects, Ru/C

ABSTRACT

The polymer reaction media and its properties can be altered by recycling a fraction of liquid products or adding alkane solvents. Less clear is whether this strategy affects hydrogenolysis. Herein, we investigated the effect of short-chain alkanes C_n consisting of n carbons ($n=8, 16$, and 32) on the upcycling of high-density polyethylene (HDPE) plastic waste to lubricant-range products over Ru/TiO₂ catalysts by multiscale simulations and experiments. First, we trained a force field for polymer/surface interactions on a Ru₂₂ nanoparticle (NP) supported on TiO₂. Using replica exchange molecular dynamics simulations, we studied the effect of small hydrocarbons on the adsorption of a surrogate polymer, C₁₄₂, on the catalyst. We found segregation of long chains (C₁₄₂) at the catalyst surface due to the enthalpy gained by adsorbing more C-C bonds of the long chains, compensating for entropic losses upon adsorption. Short-chain molecules decrease the adsorbed carbons of long chains on the Ru NP due to blocking Ru active sites. Compared to the bulk chains, competitive adsorption results in a broader, heavy-tailed distribution of end-to-end distance of adsorbed chains. Our experiments demonstrated that catalyst activity declines significantly beyond simple dilution due to changes in polymer adsorption, and tuning the reaction media by creating suitable blends impacts hydrogenolysis. Density distributions for a 50:50%wt mixture of PP and PE show that PE chains are segregated at the surface, so they are prone to C-C bond breaking much faster than PP chains. H/D exchange experiments show preferential deuteration of PE, while CH₃ groups of PP remain undeuterated. This may be explained by the preferential sorption of PE over PP, leading to specific distribution in the polymer blend.

1. Introduction

Chemical recycling of plastic waste to value-added products can complement mechanical recycling to curtail plastic waste [1]. Chemical recycling aims to develop technically feasible, economically viable, and environmentally sustainable processes [2]. Hydrogenolysis of high-density polyethylene (HDPE), low-density polyethylene (LDPE), and polypropylene (PP) over Ru- and Pt-based catalysts to lubricant range products has drawn much attention recently because of the high market volume and market share. Tennakoon et al. [3] successfully synthesized a core-shell Pt/SiO₂ catalyst in which the Pt nanoparticles (NPs) are at the edge of nanopores in a mesoporous silica shell. The catalyst yielded diesel and lubricant-range alkanes from PE. Kots et al.

studied the hydrogenolysis of PP over Ru/TiO₂ catalysts and achieved lubricant-range hydrocarbons with narrow molecular weight distributions [4].

The high activity of Ru and Pt catalysts often leads to cascade methane formation [5,6], reducing the yield to lubricants. Techno-economic analysis on the conversion of plastic waste into lubricants showed that a 90% yield to C₃₅ lubricant significantly reduced the cost by 70% (capital and operating) vs. a 60% yield [7]. Consequently, catalyst and process development to increase the lubricant yield is necessary. A fundamental understanding of interfacial phenomena at the catalyst/polymer interface is critical to achieve this goal.

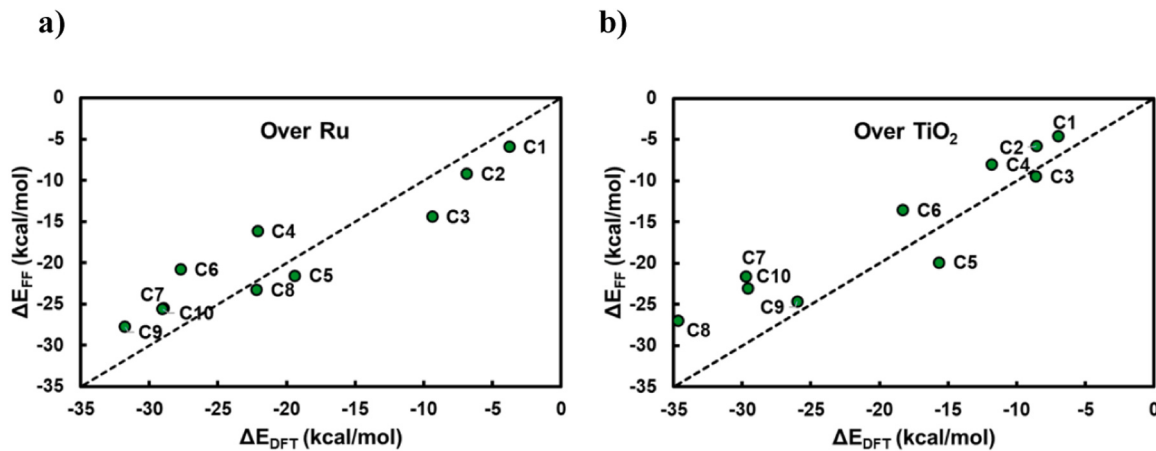
One crucial aspect of plastic depolymerization that has received little attention is the design of the reaction media. One could intentionally

* Corresponding author.

** Correspondence to: Center for Plastics Innovation, University of Delaware, Newark, DE 19716, United States.

E-mail addresses: cstavros@udel.edu (S. Caratzoulas), vlachos@udel.edu (D.G. Vlachos).





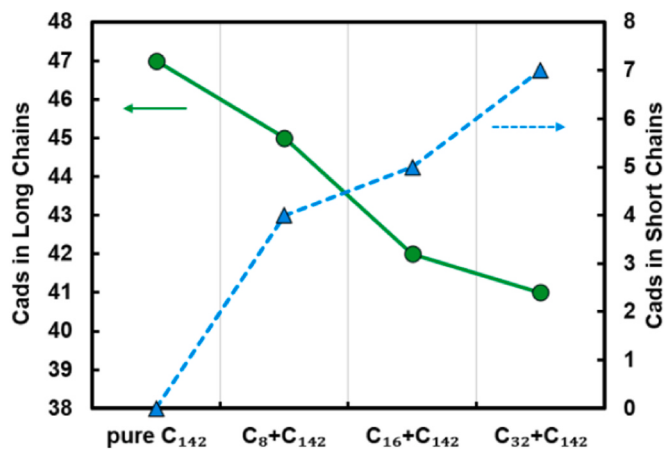


Fig. 3. Adsorbed carbons over the Ru NP in short and long chains for 50:50 wt % mixtures of $C_8:C_{142}$, $C_{16}:C_{142}$, and $C_{32}:C_{142}$ polyethylene melts at 523 K over Ru_{22}/TiO_2 catalyst. C_{ads} is adsorbed carbons on the Ru NP.

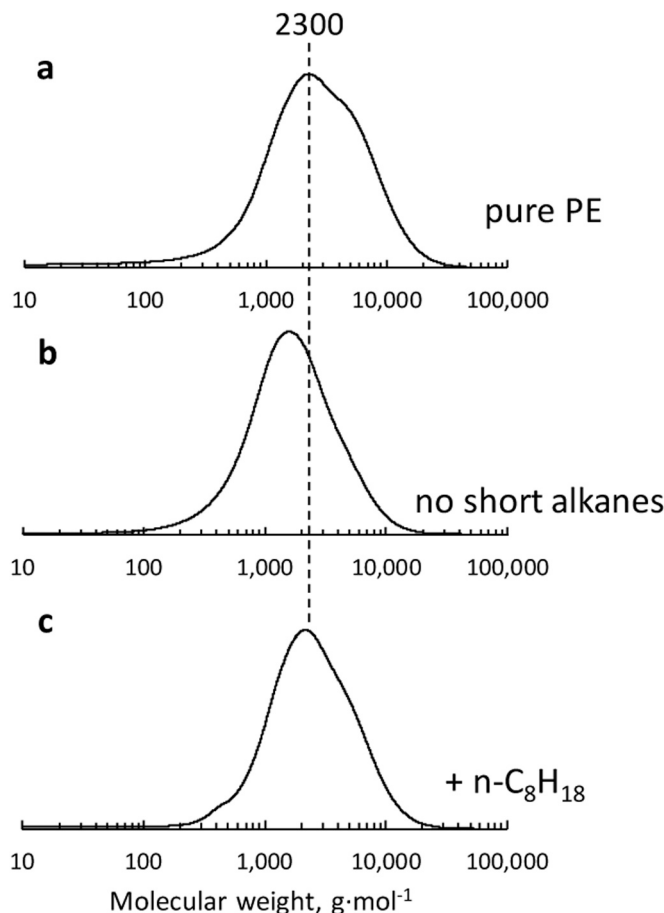


Fig. 4. GPC traces for initial PE (a), and solid residues recovered after reaction with no alkanes (b), and 50% mixture with octane (c). Reaction conditions: 250 °C, 30 bar H_2 , 0.17 h, 2 g PE, (2 g octane), 50 mg Ru/TiO_2 catalyst.

add hydrocarbons as solvents to modify the reaction media properties, such as the melt viscosity and polymer diffusivity. Recycling a suitable fraction of products can achieve the same goal without using external solvents while alleviating the need for high purity when separating the recycled stream from the product.

In this work, we employ molecular dynamics (MD) simulations to investigate the effect of co-feeding short-chain alkanes on HDPE plastic

Table 1
Experimental data on PE hydrogenolysis.

Reaction media	M_n , $kg\cdot mol^{-1}$	M_w , $kg\cdot mol^{-1}$	r_{CC} , [1] rate of C-C bond breaking, $\mu mol\cdot s^{-1}\cdot g_{cat}^{-1}$
initial, pure PE	2.22	3.86	-
no solvent	1.48	2.40	15.1
octane (n- C_8H_{18})	2.06	3.29	4.9
hexadecane (n- $C_{16}H_{34}$)	2.20	3.14	0.8
dotriacontane (n- $C_{32}H_{66}$)	1.73	2.21	17.2

¹Rate of C-C bond breaking in initial PE. Reaction conditions: 250 °C, 30 bar H_2 , 0.17 h, 2 g PE (in some cases mixed with 2 g of short alkane), 50 mg Ru/TiO_2 catalyst.

waste upcycling over Ru/TiO_2 catalysts. We hypothesize that adding short chains could alter the reactivity by modulating the adsorption and structural properties of the polymer on the Ru NPs. We develop a force field for the polymer/catalyst interfacial interactions. We simulate 50:50 wt% binary mixtures of $C_8:C_{142}$, $C_{16}:C_{142}$, and $C_{32}:C_{142}$ over a Ru_{22} nanoparticle supported on anatase $TiO_2(101)$, and we present experimental results demonstrating that small hydrocarbons in small hydrocarbon-polymer blends significantly alter the hydrogenolysis reactivity. Finally, we model a 50:50%wt mixture of polypropylene (PP) and PE and study their relative adsorption on Ru_{22}/TiO_2 as it is relevant to the recycling of mixed plastic waste; the predictions of the molecular dynamics simulations are confirmed by H/D exchange experiments.

2. Methods

2.1. Computational

Planewave periodic density functional theory (DFT) calculations were carried out in the Vienna Ab Initio Simulation Package (VASP 5.4.1) [8,9] to obtain the optimized anatase $TiO_2(101)$ slab, which is the most stable and dominant facet of TiO_2 anatase (used in the experiments). Using the supercell approach, an 8×4 unit cell with three layers ($20.90 \times 15.51 \times 9.50\text{Å}^3$), in which the bottom layer was fixed while the top two layers were relaxed, was constructed with a 25 Å vacuum layer over the surface. To model the Ru/TiO_2 catalyst, geometry optimization was performed for a Ru NP consisting of 22 atoms (Ru_{22}) supported on the optimized titania slab. This Ru NP was used since it gives us reasonable characteristics of a particle model with different facets, and its diameter ($\sim 0.8\text{ nm}$) is close to the average size of Ru particles used in experiments ($\sim 1\text{ nm}$). The frozen-core, all-electron projector augmented-wave (PAW) [10] method was utilized. The exchange-correlation energy was calculated within the generalized gradient approximation (GGA) [11] using the revised Perdew-Burke-Ernzerhof (PBE) [12-14] functional with Grimme's D3 corrections [15]. Brillouin zone integrations have been performed on a $3 \times 3 \times 1$ Γ -centered k-point grid (Γ point only used for adsorption of alkanes on Ru_{22}/TiO_2 in force-field validation), and electronic wavefunctions at each k-point were expanded using a discrete plane-wave basis set with kinetic energies limited to 450 eV. Fractional occupancies of bands were allowed within a window of 0.05 eV using Gaussian smearing. The self-consistent field (SCF) calculations converged to $1.0 \times 10^{-5}\text{ eV}$. A force criterion of $0.05\text{ eV}\text{ Å}^{-1}$ was used on relaxed atoms for geometry optimization. The geometry of the optimized NP is provided in Figure S1.

MD simulations were performed using the LAMMPS MD simulator [16]. Using the supercell approach, the clean Ru/TiO_2 surface was represented by a 16×12 slab comprising 576 Ti, 1152 O, and 22 Ru atoms with dimensions of $41.80 \times 46.52 \times 77.00\text{Å}^3$. The experimental PE melt density [17] of $\sim 0.7\text{ g}\cdot\text{cm}^{-3}$ at 523 K in the middle of the box, representing bulk PE, was achieved by packing the simulation boxes with the PE chains (see Table S1 for the number of chains used). The

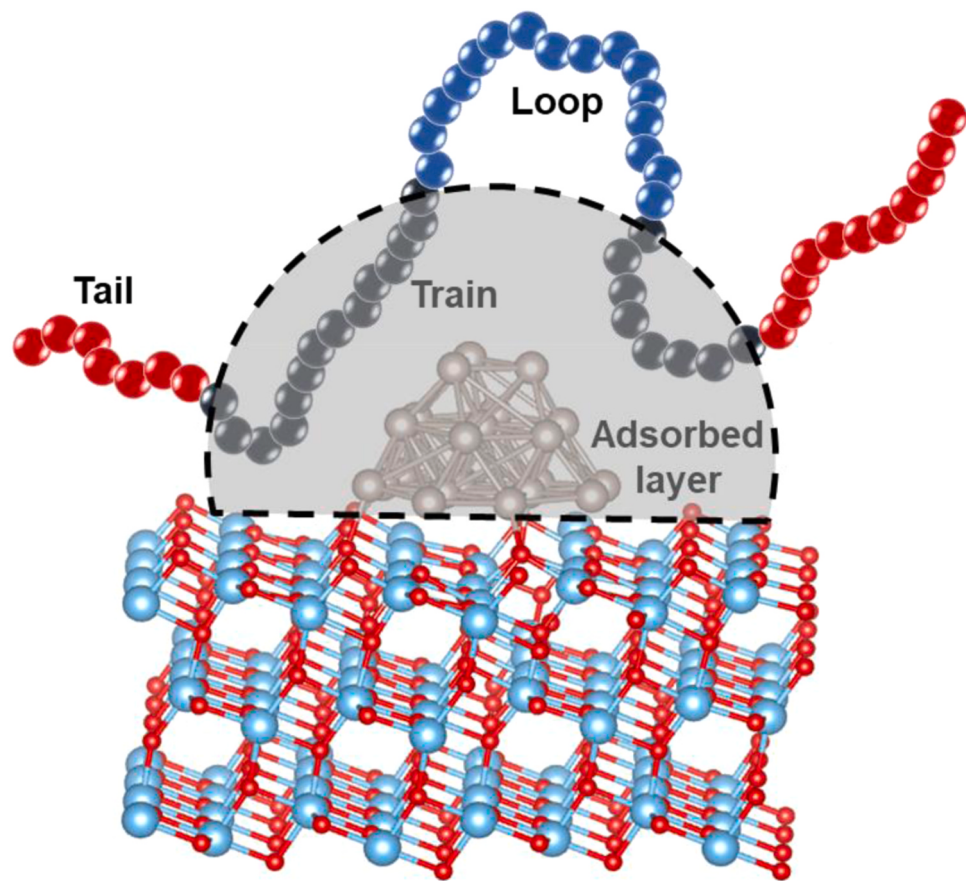


Fig. 5. Schematic representation of trains (black), tails (red), and loops (blue). Trains are selected such that the distance of every carbon atom in a train is less than 5 Å of at least one Ru surface atom to cover the first adsorption shell over Ru NP (see Lennard-Jones parameters of Ru atoms in the SI).

dimensions of the simulation boxes along the catalyst surface normal were selected so that the PE melt layer be at least 3 times as large as the equilibrium root-mean-square radius-of-gyration (R_g) of the PE chains in the bulk [18]. The PE melts were exposed to the catalyst surface on one side and vacuum on the other side along the surface normal. All catalyst atoms were kept fixed during the simulations. The PE melts were initially built in Moltemplate [19] with the OPLS-AA force field [20,21] for PE interactions. The TiO_2 -PE van-der-Waals interactions were represented by the Matsui-Akaogi (MA) force field [22,23]. To describe the Ru-PE interactions and TiO_2 -PE electrostatic interactions, we developed a force field explained in detail below (see Table S2 for all force field parameters). The geometric mixing rules, $\sigma_{ij} = \sqrt{\sigma_i \sigma_j}$ and $\epsilon_{ij} = \sqrt{\epsilon_i \epsilon_j}$ were used for cross-interaction Lennard-Jones (LJ) parameters. Simulations were carried out in the canonical ensemble (NVT) with the Nosé-Hoover thermostat with a temperature damping parameter of 100 ps [24,25]. Electrostatic interactions were accounted for by using the particle-particle particle-mesh (PPPM) method [26]. A 12 Å cutoff radius was used for the non-bonding interactions and the transition between short- and long-range electrostatic interactions.

All systems were simulated in three stages. First, the bulk PE melt was equilibrated for 1 ns in the NPT simulation. Next, the equilibrated PE melt was brought to the catalyst surface and the entire system was equilibrated for 25 ns in the NVT ensemble. Finally, the systems were equilibrated for 5 ns using Replica-Exchange MD (REMD), and data were collected for another 10 ns for 8 replicas. Details of the REMD procedures can be found elsewhere [27–30]. The swap between replicas was tried every 10 ps and the snapshots were recorded for each replica every 5 ps. The replica exchange acceptance probability was ~20%, which ensured a free random walk in the temperature space [28,31]. To

prevent possible drift or rotation of atoms by the temperature corrections, a momentum drift correction was applied every 50 ps. We used the Multi-State Bennet Acceptance Ratio estimator (MBAR), implemented in the pymbar program package [32], to obtain unbiased statistical distributions and averages.

2.2. Force field parameterization

We parameterized a force field to describe the Ru-PE interactions and TiO_2 -PE electrostatic interactions using the methodology developed by Rouse et al. [35]. First, we optimized the geometry of $\text{Ru}_{22}/\text{TiO}_2$ (8×4 unit cell) using DFT. We next performed DDEC6 partitioning of the electron density [36,37] to obtain the net atomic charges (NACs), bond orders (BOs) [38], and the cubed atomic moment (CAM) that corresponds to the volume occupied by the atom in the material; the analysis was performed in ChargeMol v3.9 [39]. Next, we used the local connectivity of atoms determined by the bond orders (we considered a threshold value of 0.25 for bonded atoms) to determine the force field atom types. We identified two Ti atom types, bulk (Ti-O6) and surface (Ti-O5/TiO6), two oxygen atom types, bulk (O-Ti3) and surface (O-Ti2), and three Ru atom types in the Ru_{22} NP, top, middle, and contact layer. Finally, we computed the averages of the net atomic charges and cubed atomic volumes. The average NACs were directly used for partial atom charges in the force field, with minor modifications providing total zero charge for the system. The average net atomic volumes were used to determine the attractive Lennard-Jones (LJ) parameter B using the theory developed by Tkachenko and Scheffler [40], and the $B(V)$ dependencies reported for each atom by Gould [41,42]. The attractive LJ parameters A were determined by simple scaling relations from the atomic volumes:

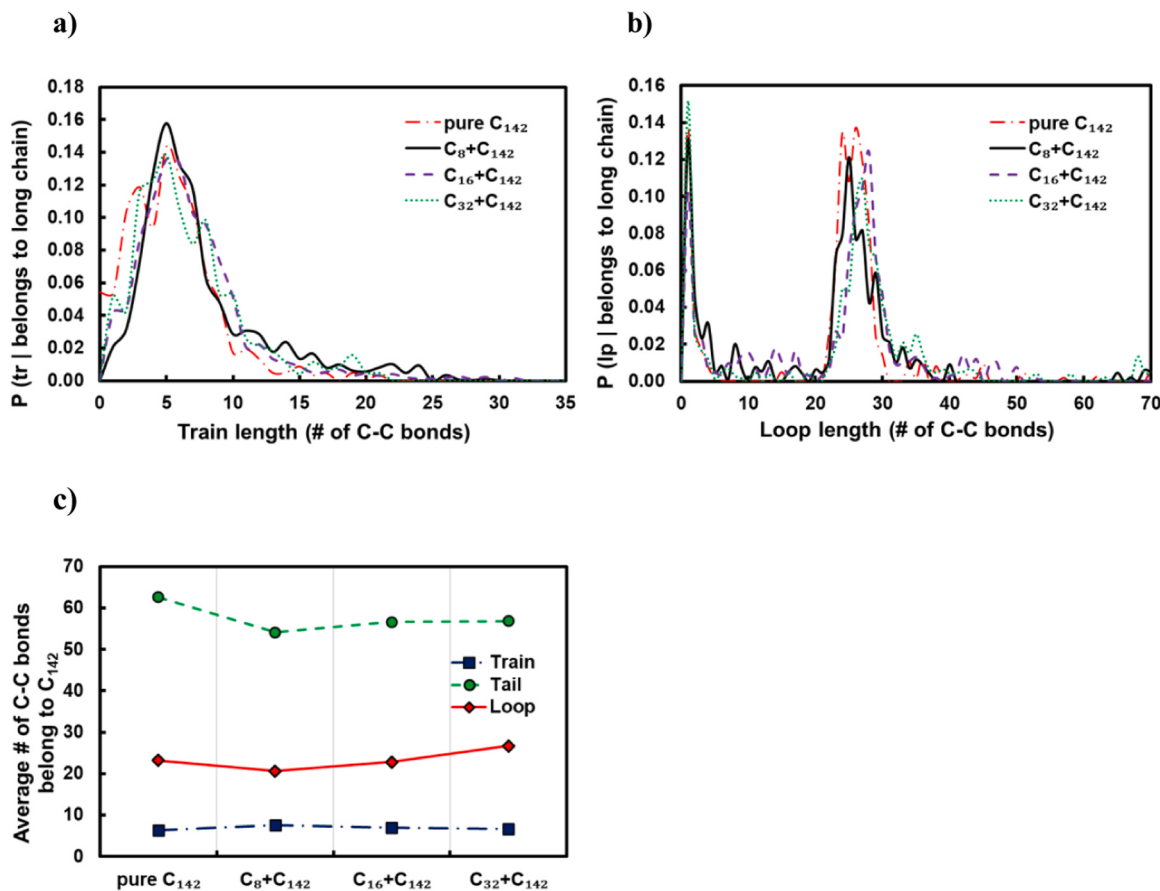


Fig. 6. Conditional probabilities of length of a) trains and b) loops in C_{142} for pure C_{142} melt and 50:50 wt% binary mixtures of C_8 , C_{16} , and C_{32} with C_{142} over $\text{Ru}_{22}/\text{TiO}_2$ catalysts at 523 K. c) Average length of trains, tails, and loops of C-C bonds in C_{142} .

$$A = \frac{1}{2} B(2R_A)^6 \quad (1)$$

wherein R_A is the effective van-der-Waals radius (equal to the minimum of the LJ potential) corresponding to the atomic volume, V . For the TiO_2 atoms, we only used the partial charges obtained from the force field. We used MA parameters for the LJ parameters of TiO_2 [22,23], which showed better accuracy during force-field validation (see Figure S2). This behavior could be attributed to the MA parameters being determined to reproduce the observed crystal structures of rutile, anatase, and brookite, and the measured elastic constants of rutile. Force field parameters for the Ru NP on anatase $\text{TiO}_2(101)$ are provided in Tables S2.

2.3. Experimental

Ru/TiO_2 catalyst with a Ru loading of 3.3 wt% was prepared [33]. The catalyst was reduced at 300 °C for 3 h in 50% H_2/He mixture, then mixed with 2 g of low-molecular-weight PE (Sigma-Aldrich, 427772) and loaded in a 50 mL Parr reactor with a magnetic stirrer. The reactor was purged 3 times with pure H_2 , charged with 30 bar H_2 , heated to 250 °C and kept at this temperature for 10 min. Then, it was quickly quenched in an ice bath. The gas phase was collected in a 1 L Tedlar gas bag. The reaction mixture was mixed with dichloromethane solvent (99.8%, Fisher), which was premixed with known amount of octacosane (>98%, TCI, P/N 00002) standard and filtered through the Whatman 1001-090 paper. The solid residue was dried overnight under ambient conditions.

The gas sample was analyzed using gas chromatography with flame ionization detector (GC-FID) on 10 m x 0.32 mm×10 μm Poraplot Q

column on an Agilent 8890 gas chromatograph. A standard gas mixture (Millipore Sigma 303100-U by Airgas) was used to calibrate retention times and FID response. An HP-1 column was used and calibrated for liquid analysis using an alkane standard solution (Supelco 04071 and 49452-U). The solid residue, made up >95% of all products, was dissolved in toluene (99.7%, Fisher) at 110 °C and separated from the catalyst powder via decanting. The toluene was then removed from the solid residue in a rotary evaporator, and the solid was further analyzed with high-temperature gel permeation chromatography (GPC) using a Tosoh HLC-8312GPC/HT instrument according to a published procedure [34]. The resulting molecular weight distribution was deconvoluted into 5 Gaussian components, and number-average and weight-average molecular weights (M_n and M_w) were calculated among all components. For samples containing hexadecane and dotriacontane (>97%, TCI), extra peaks were present in the GPC curves. The contribution of light alkanes was fitted as a separate peak and subtracted. The total content of C-C bonds in the solid residue was approximated with the following expression:

$$N_{CC} = \frac{m_i}{M_{n,i}} \left(\frac{M_{n,i}}{14} - 1 \right) \quad (2)$$

wherein [7] N_{CC} is the number of C-C bonds, m_i is the mass of the i -th solid residue, and $M_{n,i}$ is the molecular weight of the i -th solid residue, obtained from GPC analysis. For calculations in this work, m_i was assumed to be 2 g, which corresponds to 100% solid yield. The solid yield was above 95.5% in all experiments due to short reaction times. The number 14 is the molecular weight of the constituent repeating unit of polyethylene (CH_2).

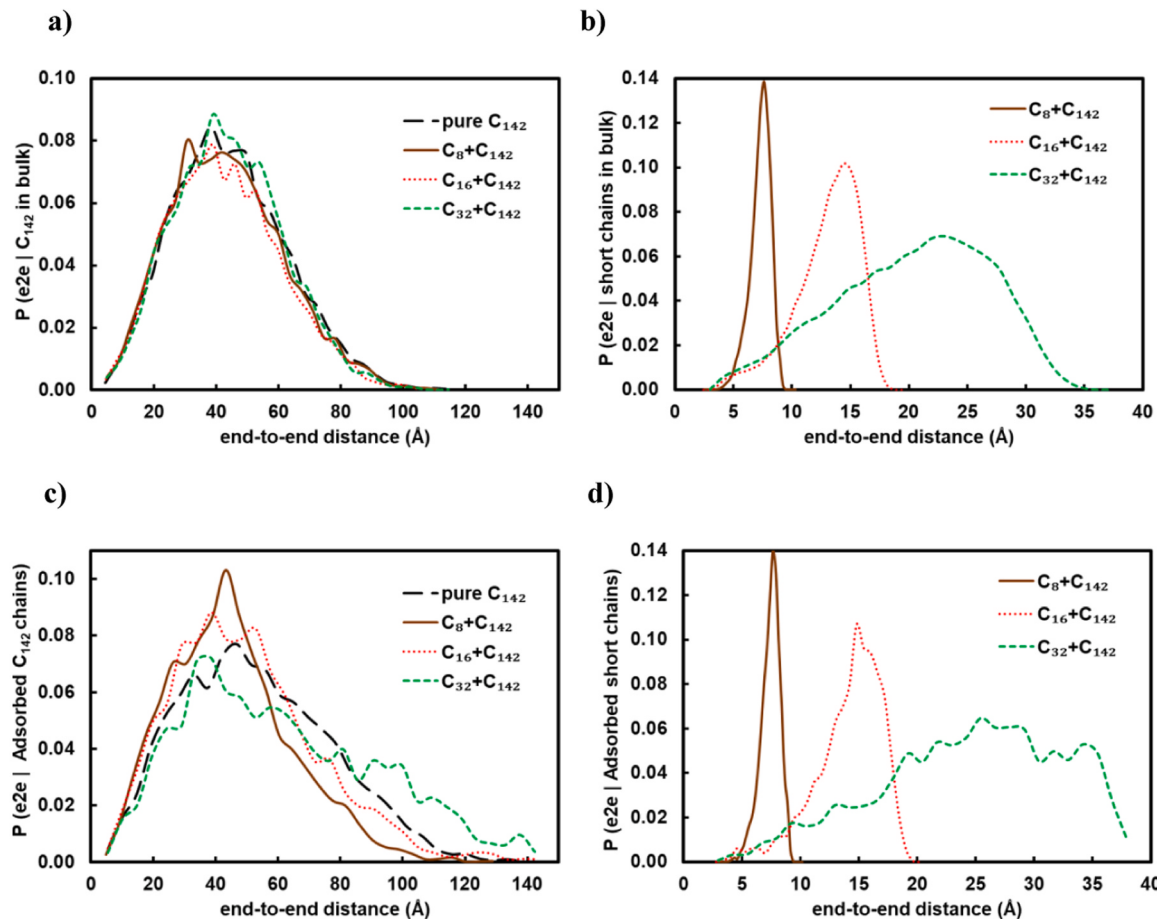


Fig. 7. Conditional probabilities of end-to-end distances (e2e) a) in C₁₄₂ chains and in the bulk that are not adsorbed on the catalyst surface, b) in short chains (C₈, C₁₆, and C₃₂ chains for C₈:C₁₄₂, C₁₆:C₁₄₂, and C₃₂:C₁₄₂ mixtures, respectively) and in the bulk, c) in C₁₄₂ chains and adsorbed, and d) in short chains and adsorbed for different polyethylene mixture melts over a Ru₂₂/TiO₂ catalyst surface model at 523 K. If a chain has at least one carbon within a 7 Å height from TiO₂ surface (see Fig. 2) or in the adsorbed layer of Ru NP (see Fig. 5), it is considered adsorbed.

2.4. The rate of C-C bond breaking was calculated as

$$r_{cc} = \frac{N_{CC}^0 - N_{CC}}{10\text{min} \bullet 0.05g_{cat}} \frac{\mu\text{mol}}{s \bullet g_{cat}} \text{ of C-C bonds}, \quad (3)$$

wherein N_{CC}^0 is the number of C-C bonds in the initial polymer. r_{cc} is normalized by the reaction time (10 min) and catalyst weight.

For the H/D exchange experiments, a Parr reactor was charged with 30 bar D₂ instead of H₂ to probe selective labeling of PE over PP. A freshly reduced catalyst was mixed with 1 g of HDPE (Sigma-Aldrich, 427985) and 1 g PP (Sigma-Aldrich, 427888). After that, the reaction continued as usual.

Attenuated total reflectance Fourier-transform IR spectra (ATR-IR) were recorded in the Nicolet Nexus spectrometer equipped with a liquid nitrogen cooled MCT detector and Smart Omni ATR accessory. The polymer mixture and solid residue were homogenized before measurements to avoid extensive phase separation. The solid was dissolved in toluene at 110 °C followed by toluene removal in a rotary evaporator. This procedure led to more uniform PP and PE distribution within the sample.

3. Results and discussion

3.1. Force field assessment

The force field of Ru₂₂/TiO₂ was validated by comparing adsorption energies (at 0 K) of C₁ to C₁₀ alkanes to DFT values. Fig. 1 shows the

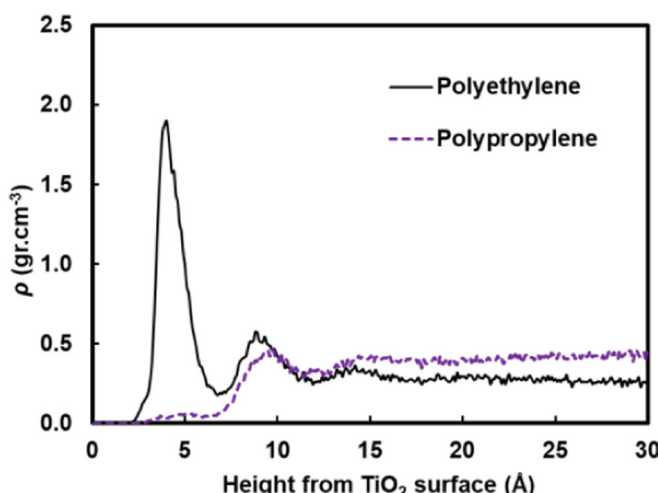


Fig. 8. Density distribution plot for a 50:50%wt mixture of PE (linear C₇₁), and PP (branched C₇₁ backbone with 34 methyl branches) over a Ru₂₂/TiO₂ catalyst surface at 523 K.

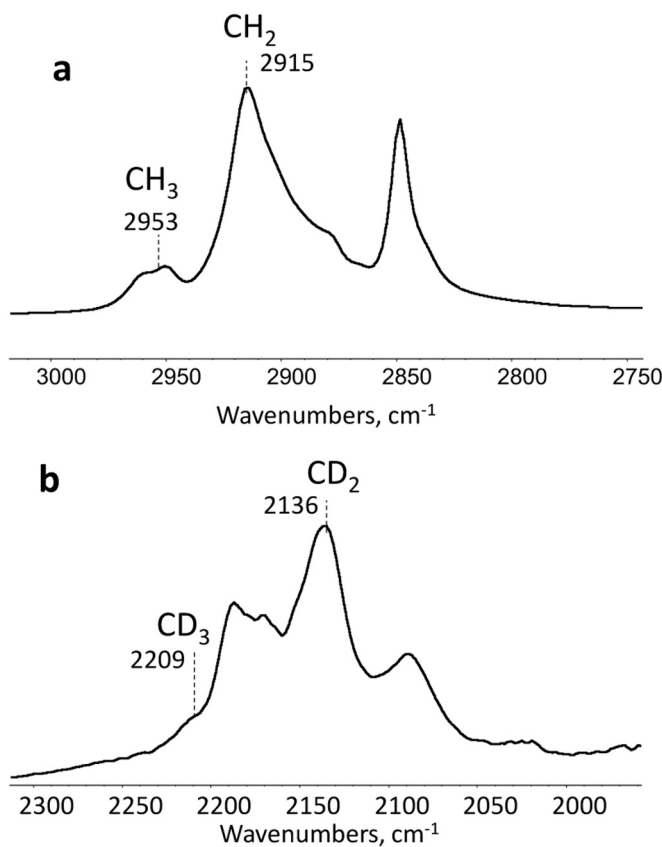


Fig. 9. ATR-FTIR spectra for PP-PE mixture after reaction. Reaction conditions: 250 °C, 30 bar D₂, 0.17 h, 1 g HDPE, 1 g PP, 50 mg Ru/TiO₂ catalyst.

force field validation results within DFT accuracy. The optimized structures of the molecules on the catalyst surface are provided in Figure S4. We also provide the force-field performance using the universal forcefield (UFF) [43] Lenard-Jones parameters for Ru atoms in Figure S3 to emphasize the need for force-field development for Ru-PE interactions.

3.2. Mixture calculations and experiments

To shed light on how solvents impact the PE reactivity, we modeled a pure C₁₄₂ melt, along with 50:50 wt% mixtures of C₈:C₁₄₂, C₁₆:C₁₄₂, and C₃₂:C₁₄₂ melts at 523 K over Ru₂₂/TiO₂ (Table S1 lists the number of molecules in each simulation). The density distributions shown in Fig. 2 indicate that long chains (C₁₄₂) segregate at the catalyst surface, in all mixtures. Increasing the short chain size from C₈ to C₁₆ and C₃₂ decreases the C₁₄₂ segregation to the catalyst surface, which is associated with the chemical similarity of the mixture components and relative entropy loss of the short vs. long chains when adsorbed to a solid surface. It has been suggested [44–47] that surface segregation is a strong function of the relative polymer-polymer and polymer-surface interactions; due to entropy, long chains near weakly attractive surfaces prefer to diffuse away, but strong polymer-surface attractive interactions can compensate for the entropic cost. Although the entropic loss of short-chain adsorption is smaller than that of long chains, the enthalpic gain by adsorption of a greater number of C-C bonds (long trains) in the long chains compensates for the entropic loss that leads to the surface segregation of long chains. Strong polymer-surface interactions bring all mixture components to the surface, and no preferred chain length surface segregation is observed. This observation agrees with our previous work in which a decrease in the strength of Pt potential led to more long-chain surface segregation in a 50:50 wt% mixture of C₂₀ and C₁₄₂ [48].

To reveal the impact of small alkane addition on adsorption, we calculated the number of adsorbed carbon atoms, C_{ads} , of short and long chains, on Ru₂₂ (see Fig. 3); a carbon atom was considered adsorbed when it was within 5 Å of a Ru. The inclusion of short chains (C₈, C₁₆, or C₃₂) in the hydrocarbon mixture decreased the C_{ads} of C₁₄₂ chains on the Ru NP. This means that short chains can block some Ru sites, potentially altering reactivity. Increasing the size of the short chain in the mixture decreased C_{ads} of C₁₄₂ and increased that of short chains. This trend agrees with the distributions in Fig. 2, in which the population of short chains on the catalyst increases with their size.

We conducted experiments for various mixtures to examine how differences in polymer binding impact the reaction outcome. We evaluated the conversion of 50:50 wt% mixtures of small alkane and polymer over a Ru/TiO₂ catalyst at 30 bar H₂ pressure at 250 °C. The solid residue constitutes 98.2–95.7% of the total product yield at this short reaction time. Therefore, GPC analysis of the remaining polymer provided quantitative insight into the PE conversion (Fig. 4, S5, and Table 1).

The starting polymer had a molecular weight distribution with two overlapping maxima and a dispersity (D) 1.74. According to GPC, the peak maximum for pure PE after the reaction shifted to a lower molecular weight than the initial polymer. In conjunction with a minor reduction in D to 1.62, all chains underwent hydrogenolysis, with heavier chains reacting more, leading to a more uniform distribution. Quantitative analyses in Table 1 indicated that pure PE's M_n was reduced by ~30%.

The addition of octane (C₈), hexadecane (C₁₆), and dotriacontane (C₃₂) leads to a lower M_n decrease, i.e., a slower evolution of the reaction. This finding is also reflected in the rate of broken C-C bonds (r_{CC}), which was calculated using Eqs. 2 and 3. Estimation of r_{CC} indicates a significant error due to the minor formation of liquid products, not considered in this calculation (Supplementary Discussion I). In the case of C₁₆ and C₃₂, a substantial amount of short alkanes was found in the solid residue (Figure S5).

M_w was more sensitive to heavier chains and decreased in all cases, indicating cleavage of the heavier part of the distribution even with light alkanes added. The average number of cleaved C-C bonds per starting polymer chain per unit of time was $1.7 \times 10^{-2} - 8.5 \times 10^{-4} \text{ s}^{-1} \cdot g_{cat}^{-1}$ depending on the alkane. During 10 min, each chain was cleaved only 0.5 times without added alkanes. This cleavage rate corresponds to a minor fraction of chains having higher reactivity than the rest. So heavier chains dominate active sites and cleave initially with the attendant gradual shift of the whole distribution to lower sizes. This behavior is consistent with previous reports on Ru- and Ni-catalyzed PE conversion [49,50].

Literature data indicate increased polymer self-diffusivity when adding small molecules. For the octane-PE mixture, the polymer self-diffusion coefficient (D_s) increases fivefold, from 7.6×10^{-6} to $1.6 \times 10^{-6} \text{ cm}^2 \cdot \text{s}^{-1}$ [51]. An increase in D_s according to our data (Table 1) does not lead to increased reaction rate, indicating bulk diffusion does not limit the reaction. The observed reaction rate decrease with alkane addition is attributed to competitive adsorption with the polymer, as shown in the MD simulations. Indeed, small octane or hexadecane molecules bind to the Ru NPs, decreasing the polymer adsorbed on the active sites. Furthermore, the alkanes dilute the polymer melt and reduce the overall polymer concentration. Apparent reaction rates (r_{CC}) were normalized per PE concentration in the melt and polymer molar fraction in the adsorbed layer (Table S3). Interestingly, the results demonstrate that the catalyst activity declines beyond simple effect of dilution (see Supplementary Discussion I). The polymer binding to the Ru surface is altered by short alkanes, which affects reaction rate. Formally, changes in polymer reactivity are expressed in very low polymer activity coefficients within the adsorbed layer (Supplementary Discussion II).

The addition of octane or hexadecane leads to comparable polymer

molar fractions in the adsorbed layer of 0.44–0.49, but the calculated r_{CC} reaction rate in these cases differs 6x. The minor inhibiting effect of octane, compared to hexadecane, can be attributed to high octane vapor pressure under reaction conditions, which would lead to lower effective octane content in the melt.

For longer dotriacontane (C_{32}), we find a slight change in M_n and r_{CC} in comparison to the alkane-free case. Hence, despite dilution with dotriacontane, we do observe only slight inhibition of hydrogenolysis. Apparently, polymer reactivity depends on having short alkane size, and it was studied in more detail with simulations.

3.3. Structural properties of polymers over Ru/TiO_2 catalysts

We used the standard definitions of trains, tails, and loops to analyze the polymer structures of PE chains on the Ru NP [52,53]. An illustration of these conformational features is provided in Fig. 5: contiguous backbone carbon atoms on the Ru surface define a train; two successive trains are connected by a loop, whose carbon atoms do not lie on the Ru surface; and a tail succeeds a train that is not followed by another one, *i.e.*, it is part of a chain extending into the melt. The number of C-C bonds defines the length of a train, tail, or loop. In our analysis, trains are selected such that the distance of every carbon atom in a train is less than 5 Å from at least one Ru surface atom to cover the first adsorption shell over the Ru NP (see Lennard-Jones parameters of Ru atoms in the SI). These features enable us to statistically predict which and how many C-C bonds lie close to the Ru NP to qualitatively relate the structure of the polymer at the catalyst surface to reactivity.

The conditional probability of trains in the long chain plotted in Fig. 6a shows a peak at train length of ~5 for all simulations independent of short-chain alkane size in the mixture. This intuitive finding showcases that the size of Ru NP determines the number of consecutive adsorbed C-C bonds (trains). Adding a short chain to C_{142} in a 50:50 wt% mixture makes the loop distributions broader and less structured. It also slightly alters the peak formed at a loop length of ~25 for the pure C_{142} and C_8+C_{142} simulations vs. that of ~28 for the $C_{16}+C_{142}$ and $C_{32}+C_{142}$ simulations. Finally, a longer loop forms when increasing the size of the short chain in the mixture (see Fig. 6c).

The end-to-end distance (e2e) of chains was used to study the impact of the catalyst surface on the conformations of polymer melts. We distinguished adsorbed chains on the catalyst surface from those in the bulk and plotted the conditional probabilities of e2e of short and long chains. Analysis for polymer melts over the Ru_{22}/TiO_2 catalyst surface provided in Fig. 7 shows a broader and heavy-tailed distribution of adsorbed chains compared to chains in the bulk. Adsorbed chains have at least one carbon within 7 Å of the TiO_2 surface (see Figs. 2) or 5 Å from the Ru NP surface (see Fig. 5). Adding short chains to pure C_{142} melts does not impact the e2e of chains in the bulk (see Fig. 7a). Furthermore, short chains in the mixture make the e2e distribution in long chains (C_{142}) broader and less structured.

3.4. PP and PE mixtures

An advantage of chemical recycling compared to mechanical recycling is its applicability to mixed-plastics waste streams. These can undergo selective catalytic fractionation chemistry in which sequential steps selectively deconstruct individual plastic materials [2]. Here, we have modeled a 50:50%wt mixture of polypropylene (PP) and PE to study their relative adsorption on Ru_{22}/TiO_2 . C_7 chains represent PE and C_{71} backbones branched with 34 methyl group represent PP chains. The density distribution in Fig. 8 clearly shows that PE chains segregate to the surface, potentially becoming available for C-C bond breaking compared to PP chains. To confirm this finding, we performed H/D exchange experiments. H/D exchange in polyolefins is highly sensitive to polymer-catalyst interactions [54,55]. A mixture of PP and HDPE with comparable M_n reacted over Ru/TiO_2 catalyst for 10 min in D_2 gas to convert C-H bonds to C-D bonds, while avoiding complete H/D

averaging (Fig. 9).

ATR spectra in the CH stretching region of the initial polymers mixture have peaks for $\nu_{as}(CH_3)$ at ~2953 cm⁻¹, characteristic of PP [56]. A broad and intense peak at 2915 cm⁻¹ corresponds to $\nu_{as}(CH_2)$ in PE and PP [57], and a sharper signal at 2848 cm⁻¹ is due to $\nu_s(CH_2)$, also expected for both polymers. The CD stretching region of the solid residue after reaction has peaks at 2187, 2136 and 2088 cm⁻¹ due to deuterated CD_2 groups, which match the spectrum of deuterated HDPE (Figure S7). On the other hand, the peak at ~2209 cm⁻¹, a typical of $\nu_{as}(CD_3)$ in PP [56], is absent. This shows preferential deuteration of PE, while CH_3 groups of PP remain undeuterated. This may be explained by the preferential sorption of PE over PP, leading to specific D distribution of the polymer blend.

4. Conclusions

We investigated the effect of short-chain alkanes on the upcycling of HDPE plastic waste over Ru/TiO_2 catalysts. We first developed a force field for Ru/TiO_2 catalysts, which was validated by comparing adsorption energies (at 0 K) of C_1 to C_{10} alkanes to DFT values. Unlike previous simulations on infinitely large uniform surfaces, such a force field enabled us to perform the first simulations for a finite metal catalyst particle size on a support and account for polymer-catalyst and polymer-support interactions. Next, we modeled 50:50 wt% binary mixtures of C_n ($n=8, 16$, and 32) with C_{142} over Ru_{22} nanoparticles supported on anatase $TiO_2(101)$.

Density distributions suggest long chains (C_{142}) segregate at the catalyst surface due to the enthalpic gain by adsorption of a greater number of C-C bonds (long trains) of long chains, which compensates for entropic losses when bulk chains adsorb to the surface. The addition of short chains (C_8, C_{16} , or C_{32}) to the polymer melt decrease the adsorbed carbons of C_{142} chains on the Ru NP due to blocking Ru active sites and potentially altering reactivity.

Experimental data demonstrate that catalyst activity declines beyond simple dilution. The addition of octane or hexadecane leads to comparable polymer molar fractions in the adsorbed layer of 0.44–0.49, but the reaction rate decreases 6x. Small alkanes change the polymer adsorption, but it is hard to capture experimentally these phenomena. Molecular simulations can provide such insights in future work. Additional simulation and experiments can better explain how branching of short alkane will impact the properties of the polymer.

Structural analysis of adsorbed polymers on the Ru nanoparticle indicates that the trains of long chains have a most probable train length of ~5, independent of short-chain alkane size. This length is dictated by the Ru NP. The average length of loops increases when increasing the size of the short chains. The end-to-end distance (e2e) shows a broader and heavy-tailed distribution for adsorbed chains compared to those in the bulk. Short chains in the melts do not impact the e2e of bulk chains but makes the distribution in long chains (C_{142}) broader and less structured. The work can be extended to mixed plastics. For example, we showed that PE preferentially adsorbs at the catalyst surface over PP in a 50:50%wt mixture of PE and PP.

Our results demonstrate that interfacial polymer/surface interactions are crucial to deconstruction. Small alkanes blended with polymers tune the reaction media bulk properties. Importantly, they also change the adsorption of polymers and, thus, reactivity. Molecular simulations are instrumental in providing insights and designing the reaction media.

CRediT authorship contribution statement

Dionisios G Vlachos: Writing – review & editing, Supervision, Project administration, Funding acquisition, Conceptualization. **Mehdi Zare:** Writing – review & editing, Writing – original draft, Methodology, Investigation, Formal analysis, Data curation, Conceptualization. **LaShanda Korley:** Writing – review & editing, Supervision, Funding

acquisition. **Stavros Caratzoulas:** Writing – review & editing, Supervision, Project administration, Funding acquisition, Conceptualization. **Zachary Hinton:** Writing – original draft, Data curation, Conceptualization. **Thomas Epps, III:** Writing – review & editing, Supervision, Funding acquisition. **Pavel Kots:** Writing – review & editing, Writing – original draft, Methodology, Investigation, Formal analysis, Data curation.

Declaration of Competing Interest

The authors declare no conflict of interest.

Data Availability

Data will be made available on request.

Acknowledgments

This work was intellectually led and supported as part of the Center for Plastics Innovation, an Energy Frontier Research Center funded by the US Dept. of Energy, Office of Science, Office of Basic Energy Sciences under award number DE-SC0021166. The data analysis was supported by the National Science Foundation under Grant No. 2134471.

Appendix A. Supporting information

Supplementary data associated with this article can be found in the online version at [doi:10.1016/j.apcatb.2024.123969](https://doi.org/10.1016/j.apcatb.2024.123969).

References

- [1] Tsakona, M.; Baker, E.; Rucevska, I.; Maes, T.; Appelquist, L.R.; Macmillan-Lawler, M.; Harris, P.; Raubenheimer, K.; Langgaard, R.; Savelli-Soderberg, H.; et al. Drowning in plastics—marine litter and plastic waste vital graphics; United Nations Environment Programme, 2021.
- [2] S.R. Nicholson, J.E. Rorrer, A. Singh, M.O. Konev, N.A. Rorrer, A.C. Carpenter, A. J. Jacobsen, Y. Román-Leshkov, G.T. Beckham, The critical role of process analysis in chemical recycling and upcycling of waste plastics, *Annu. Rev. Chem. Biomol. Eng.* **13** (1) (2022) 301–324, <https://doi.org/10.1146/annurev-chembioeng-100521-085846>.
- [3] A. Tennakoon, X. Wu, A.L. Paterson, S. Patnaik, Y. Pei, A.M. LaPointe, S.C. Ammal, R.A. Hackler, A. Heyden, I.I. Slowing, et al., Catalytic upcycling of high-density polyethylene via a processive mechanism, *Nat. Catal.* **3** (11) (2020) 893–901, <https://doi.org/10.1038/s41929-020-00519-4>.
- [4] P.A. Kots, S. Liu, B.C. Vance, C. Wang, J.D. Sheehan, D.G. Vlachos, Polypropylene plastic waste conversion to lubricants over Ru/TiO₂ catalysts, *ACS Catal.* **11** (13) (2021) 8104–8115, <https://doi.org/10.1021/acscatal.1c00874>.
- [5] C. Wang, K. Yu, B. Sheludko, T. Xie, P.A. Kots, B.C. Vance, P. Kumar, E.A. Stach, W. Zheng, D.G. Vlachos, A general strategy and a consolidated mechanism for low-methane hydrogenolysis of polyethylene over ruthenium, *Appl. Catal. B: Environ.* **319** (2022) 121899, <https://doi.org/10.1016/j.apcatb.2022.121899>.
- [6] P.A. Kots, B.C. Vance, D.G. Vlachos, Polyolefin plastic waste hydroconversion to fuels, lubricants, and waxes: a comparative study, *10.1039/D1RE00447F, React. Chem. Eng.* **7** (1) (2022) 41–54, <https://doi.org/10.1039/D1RE00447F>.
- [7] V. Cappello, P. Sun, G. Zang, S. Kumar, R. Hackler, H.E. Delgado, A. Elgawainy, M. Delferro, T. Krause, Conversion of plastic waste into high-value lubricants: techno-economic analysis and life cycle assessment, *10.1039/D2GC01840C, Green. Chem.* **24** (16) (2022) 6306–6318, <https://doi.org/10.1039/D2GC01840C>.
- [8] G. Kresse, J. Furthmüller, Efficiency of ab-initio total energy calculations for metals and semiconductors using a plane-wave basis set, in: *Comp. Mater. Sci.*, **6**, 1996, pp. 15–50. DOI 10.1016/0927-0256(96)00008-0.
- [9] G. Kresse, J. Furthmüller, Efficient iterative schemes for ab initio total-energy calculations using a plane-wave basis set, in: *Phys Rev B*, **54**, 1996, pp. 11169–11186. DOI 10.1103/PhysRevB.54.11169.
- [10] P.E. Blöchl, Projector augmented-wave method, *Phys. Rev. B* **50** (24) (1994) 17953–17979, <https://doi.org/10.1103/PhysRevB.50.17953>.
- [11] J.P. Perdew, K. Burke, M. Ernzerhof, Generalized gradient approximation made simple, in: *Phys Rev Lett.*, **77**, 1996, pp. 3865–3868. DOI 10.1103/PhysRevLett.77.3865.
- [12] J.P. Perdew, W. Yue, Accurate and simple density functional for the electronic exchange energy – generalized gradient approximation, in: *Phys Rev B*, **33**, 1986, pp. 8800–8802. DOI 10.1103/PhysRevB.33.8800.
- [13] J.P. Perdew, Y. Wang, Accurate and Simple Analytic Representation of the Electron-Gas Correlation-Energy, in: *Phys Rev B*, **45**, 1992, pp. 13244–13249. DOI 10.1103/PhysRevB.45.13244.
- [14] B. Hammer, L.B. Hansen, J.K. Nørskov, Improved adsorption energetics within density-functional theory using revised Perdew-Burke-Ernzerhof functionals, *Phys. Rev. B* **59** (11) (1999) 7413–7421, <https://doi.org/10.1103/PhysRevB.59.7413>.
- [15] S. Grimme, J. Antony, S. Ehrlich, H. Krieg, A consistent and accurate ab initio parametrization of density functional dispersion correction (DFT-D) for the 94 elements H–Pu, *J. Chem. Phys.* **132** (15) (2010) 154104, <https://doi.org/10.1063/1.3382344>.
- [16] A.P. Thompson, H.M. Aktulga, R. Berger, D.S. Bolintineanu, W.M. Brown, P. S. Crozier, in 't Veld, P. J.; Kohlmeier, A.; Moore, S. G.; Nguyen, T. D.; et al. LAMMPS - a flexible simulation tool for particle-based materials modeling at the atomic, meso, and continuum scales, *Comput. Phys. Commun.* **271** (2022) 108171 <https://doi.org/10.1016/j.cpc.2021.108171>.
- [17] G.T. Dee, T. Ougizawa, D.J. Walsh, The pressure-volume-temperature properties of polyethylene, poly(dimethyl siloxane), poly(ethylene glycol) and poly(propylene glycol) as a function of molecular weight, *Polymer* **33** (16) (1992) 3462–3469, [https://doi.org/10.1016/0032-3861\(92\)91104-A](https://doi.org/10.1016/0032-3861(92)91104-A).
- [18] K.C. Daoulas, V.A. Harmansdari, V.G. Mavrantzas, Detailed atomistic simulation of a polymer melt/solid interface: structure, density, and conformation of a thin film of polyethylene melt adsorbed on graphite, *Macromolecules* **38** (13) (2005) 5780–5795, <https://doi.org/10.1021/ma050176r>.
- [19] A.I. Jewett, D. Stelter, J. Lambert, S.M. Saladi, O.M. Roscioni, M. Ricci, L. Autin, M. Maritan, S.M. Bashusqeh, T. Keyes, et al., Moltemplate: a tool for coarse-grained modeling of complex biological matter and soft condensed matter physics, *J. Mol. Biol.* **433** (11) (2021) 166841, <https://doi.org/10.1016/j.jmb.2021.166841>.
- [20] W.L. Jorgensen, J. Tirado-Rives, Molecular modeling of organic and biomolecular systems using BOSS and MCPRO, *J. Comput. Chem.* **26** (16) (2005) 1689–1700, <https://doi.org/10.1002/jcc.20297>.
- [21] J.A. Rackers, Z. Wang, C. Lu, M.L. Laury, L. Lagardère, M.J. Schnieders, J.-P. Piquemal, P. Ren, J.W. Ponder, Tinker 8: software tools for molecular design, *J. Chem. Theory Comput.* **14** (10) (2018) 5273–5289, <https://doi.org/10.1021/acs.jctc.8b00529>.
- [22] M. Matsui, M. Akaogi, Molecular dynamics simulation of the structural and physical properties of the four polymorphs of TiO₂, *Mol. Simul.* **6** (4–6) (1991) 239–244, <https://doi.org/10.1080/08927029108022432>.
- [23] B. Luan, T. Huynh, R. Zhou, Simplified TiO₂ force fields for studies of its interaction with biomolecules, *J. Chem. Phys.* **142** (23) (2015) 234102, <https://doi.org/10.1063/1.4922618>.
- [24] S. Nosé, A unified formulation of the constant temperature molecular dynamics methods, *J. Chem. Phys.* **81** (1) (1984) 511–519, <https://doi.org/10.1063/1.447334>.
- [25] W.G. Hoover, Canonical dynamics: equilibrium phase-space distributions, *Phys. Rev. A* **31** (3) (1985) 1695–1697, <https://doi.org/10.1103/PhysRevA.31.1695>.
- [26] R.W. Hockney, J.W. Eastwood, *Computer Simulation Using Particles*, Adam Hilger, 1989.
- [27] K. Hukushima, K. Nemoto, Exchange Monte Carlo method and application to spin glass simulations, *J. Phys. Soc. Jpn.* **65** (6) (1996) 1604–1608, 10.1143/JPSJ.65.1604 (accessed 2022/04/21).
- [28] Y. Sugita, Y. Okamoto, Replica-exchange molecular dynamics method for protein folding, *Chem. Phys. Lett.* **314** (1) (1999) 141–151, [https://doi.org/10.1016/S0009-2614\(99\)01123-9](https://doi.org/10.1016/S0009-2614(99)01123-9).
- [29] Y. Sugita, A. Kitao, Y. Okamoto, Multidimensional replica-exchange method for free-energy calculations, *J. Chem. Phys.* **113** (15) (2000) 6042–6051, <https://doi.org/10.1063/1.1308516>.
- [30] D.J. Earl, M.W. Deem, Parallel tempering: Theory, applications, and new perspectives, *10.1039/B509983H, Phys. Chem. Chem. Phys.* **7** (23) (2005) 3910–3916, <https://doi.org/10.1039/B509983H>.
- [31] A. Kone, D.A. Kofke, Selection of temperature intervals for parallel-tempering simulations, *J. Chem. Phys.* **122** (20) (2005) 206101, <https://doi.org/10.1063/1.1917749>.
- [32] M.R. Shirts, J.D. Chodera, Statistically optimal analysis of samples from multiple equilibrium states, *J. Chem. Phys.* **129** (12) (2008) 124105, <https://doi.org/10.1063/1.2978177>.
- [33] P.A. Kots, T. Xie, B.C. Vance, C.M. Quinn, M.D. de Mello, J.A. Boscoboinik, C. Wang, P. Kumar, E.A. Stach, N.S. Marinkovic, et al., Electronic modulation of metal-support interactions improves polypropylene hydrogenolysis over ruthenium catalysts, *Nat. Commun.* **13** (1) (2022) 5186, <https://doi.org/10.1038/s41467-022-32934-5>.
- [34] Z.R. Hinton, P.A. Kots, M. Soukaseum, B.C. Vance, D.G. Vlachos, T.H. Epps, L.T. J. Korley, Antioxidant-induced transformations of a metal-acid hydrocracking catalyst in the deconstruction of polyethylene waste, *10.1039/D2GC02503E, Green. Chem.* **24** (19) (2022) 7332–7339, <https://doi.org/10.1039/D2GC02503E>.
- [35] I. Rouse, D. Power, E.G. Brandt, M. Schneemilch, K. Kotsis, N. Quirke, A. P. Lyubartsev, V. Lobaskin, First principles characterisation of bio-nano interface, *10.1039/D1CP0116B, Phys. Chem. Chem. Phys.* **23** (24) (2021) 13473–13482, <https://doi.org/10.1039/D1CP0116B>.
- [36] T.A. Manz, N.G. Limas, Introducing DDEC6 atomic population analysis: part 1. Charge partitioning theory and methodology, *10.1039/C6RA04656H, RSC Adv.* **6** (53) (2016) 47771–47801, <https://doi.org/10.1039/C6RA04656H>.
- [37] N.G. Limas, T.A. Manz, Introducing DDEC6 atomic population analysis: part 2. Computed results for a wide range of periodic and nonperiodic materials, *10.1039/C6RA05507A, RSC Adv.* **6** (51) (2016) 45727–45747, <https://doi.org/10.1039/C6RA05507A>.
- [38] T.A. Manz, Introducing DDEC6 atomic population analysis: part 3. Comprehensive method to compute bond orders, *10.1039/C7RA07400J, RSC Adv.* **7** (72) (2017) 45552–45581, <https://doi.org/10.1039/C7RA07400J>.

[39] N.G. Limas, T.A. Manz, Introducing DDEC6 atomic population analysis: part 4. Efficient parallel computation of net atomic charges, atomic spin moments, bond orders, and more, *10.1039/C7RA11829E*, *RSC Adv.* **8** (5) (2018) 2678–2707, <https://doi.org/10.1039/C7RA11829E>.

[40] A. Tkatchenko, M. Scheffler, Accurate molecular Van Der Waals interactions from ground-state electron density and free-atom reference data, *Phys. Rev. Lett.* **102** (7) (2009) 073005, <https://doi.org/10.1103/PhysRevLett.102.073005>.

[41] T. Gould, How polarizabilities and C6 coefficients actually vary with atomic volume, *J. Chem. Phys.* **145** (8) (2016) 084308, <https://doi.org/10.1063/1.4961643>.

[42] T. Gould, T. Bučko, C6 coefficients and dipole polarizabilities for all atoms and many ions in rows 1–6 of the periodic table, *J. Chem. Theory Comput.* **12** (8) (2016) 3603–3613.

[43] A.K. Rappe, C.J. Casewit, K.S. Colwell, W.A. Goddard III, W.M. Skiff, UFF, a full periodic table force field for molecular mechanics and molecular dynamics simulations, *J. Am. Chem. Soc.* **114** (25) (1992) 10024–10035, <https://doi.org/10.1021/ja00051a040>.

[44] A. Yethiraj, S. Kumar, A. Hariharan, K.S. Schweizer, Surface segregation in polymer blends due to stiffness disparity, *J. Chem. Phys.* **100** (6) (1994) 4691–4694, <https://doi.org/10.1063/1.466252>.

[45] A. Yethiraj, Entropic and enthalpic surface segregation from blends of branched and linear polymers, *Phys. Rev. Lett.* **74** (11) (1995) 2018–2021, <https://doi.org/10.1103/PhysRevLett.74.2018>.

[46] U. Steiner, J. Klein, E. Eiser, A. Budkowski, L.J. Fetters, Complete wetting from polymer mixtures, *Science* **258** (5085) (1992) 1126–1129, <https://doi.org/10.1126/science.258.5085.1126>.

[47] M. Sikka, N. Singh, A. Karim, F.S. Bates, S.K. Satija, C.F. Majkrzak, Entropy-driven surface segregation in block copolymer melts, *Phys. Rev. Lett.* **70** (3) (1993) 307–310, <https://doi.org/10.1103/PhysRevLett.70.307>.

[48] M. Zare, P.A. Kots, S. Caratzoulas, D.G. Vlachos, Conformations of polyolefins on platinum catalysts control product distribution in plastics recycling, *10.1039/D2SC04772A*, *Chem. Sci.* **14** (8) (2023) 1966–1977, <https://doi.org/10.1039/D2SC04772A>.

[49] B.C. Vance, P.A. Kots, C. Wang, J.E. Granite, D.G. Vlachos, Ni/SiO₂ catalysts for polyolefin deconstruction via the divergent hydrogenolysis mechanism, *Appl. Catal. B: Environ.* **322** (2023) 122138, <https://doi.org/10.1016/j.apcatb.2022.122138>.

[50] C. Wang, T. Xie, P.A. Kots, B.C. Vance, K. Yu, P. Kumar, J. Fu, S. Liu, G. Tsilomelekis, E.A. Stach, et al., Polyethylene hydrogenolysis at mild conditions over ruthenium on tungstated zirconia, *JACS Au* **1** (9) (2021) 1422–1434, <https://doi.org/10.1021/jacsau.1c00200>.

[51] E. von Meerwall, E.J. Feick, R. Ozisik, W.L. Mattice, Diffusion in binary liquid n-alkane and alkane-polyethylene blends, *J. Chem. Phys.* **111** (2) (1999) 750–757, [10.1063/1.479354](https://doi.org/10.1063/1.479354) (accessed 6/16/2023).

[52] A.N. Semenov, J. Bonet-Avalos, A. Johner, J.F. Joanny, Adsorption of polymer solutions onto a flat surface, *Macromolecules* **29** (6) (1996) 2179–2196, <https://doi.org/10.1021/ma950712n>.

[53] C.A.J. Hoeve, E.A. DiMarzio, P. Peyser, Adsorption of polymer molecules at low surface coverage, *J. Chem. Phys.* **42** (7) (1965) 2558–2563, <https://doi.org/10.1063/1.1696332>.

[54] S.P. Ertel, C.E. Onuoha, H. Wang, M.A. Hillmyer, T.M. Reineke, T.P. Lodge, F. S. Bates, Hydrogenolysis of linear low-density polyethylene during heterogeneous catalytic hydrogen–deuterium exchange, *Macromolecules* **53** (14) (2020) 6043–6055, <https://doi.org/10.1021/acs.macromol.0c00696>.

[55] J.C. Nicholson, B. Crist, Hydrogen-deuterium exchange for labeling polyethylene, *Macromolecules* **22** (4) (1989) 1704–1708.

[56] C.Y. Liang, M.R. Lytton, C.J. Boone, Infrared spectra of crystalline and stereoregular polymers. II. Carbon–hydrogen and carbon–deuterium stretching frequencies of polypropylene and deuterated polypropylenes, *J. Polym. Sci.* **47** (149) (1960) 139–148, <https://doi.org/10.1002/pol.1960.1204714912>.

[57] E. Andreassen, Infrared and Raman spectroscopy of polypropylene, in: J. Karger-Kocsis (Ed.), *An A-Z reference, Polypropylene*, Springer Netherlands, 1999, pp. 320–328.